Visualization of Brain Microstructure through Spherical Harmonics Illumination of High Fidelity Spatio-Angular Fields

Sujal Bista, Jiachen Zhuo, Rao P. Gullapalli, and Amitabh Varshney, *Fellow*, *IEEE*

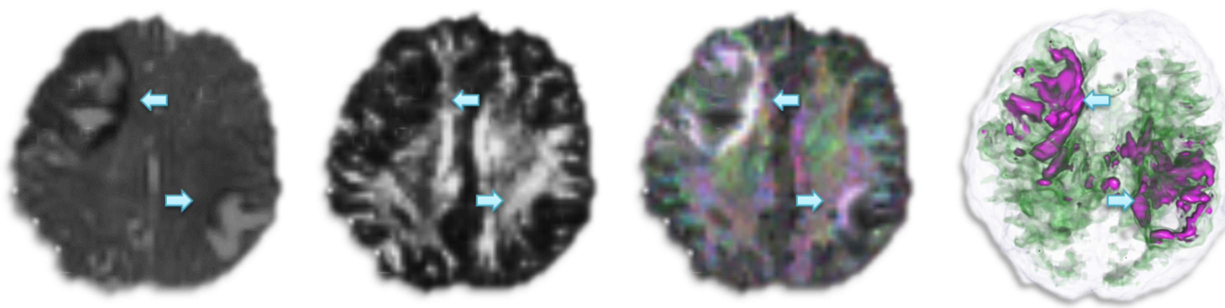

(a) (b) (c) (d)

Fig. 1. Using spherical harmonics lighting functions described in this paper, we visualize spatio-angular fields. In this figure, we use the dataset of a patient suffering from traumatic brain injury. In traditional diffusion tensor imaging, the region around the injury does not exhibit a high contrast, as seen in the mean diffusion in image 1(a) and fractional anisotropy in image 1(b). The results of our approach can be seen in images 1(c) and 1(d) that can better depict the detailed structure around the injury site facilitating a more informed assessment of the extent of injury. Figure 1(c) shows the structural changes through color and intensity using spherical-harmonic lighting over the diffusion kurtosis tensors for each pixel. Figure 1(d) shows the results of volume rendering where opacity and color are determined by spherical harmonic illumination of the diffusion kurtosis tensors for each voxel.

Abstract— Diffusion kurtosis imaging (DKI) is gaining rapid adoption in the medical imaging community due to its ability to measure the non-Gaussian property of water diffusion in biological tissues. Compared to traditional diffusion tensor imaging (DTI), DKI can provide additional details about the underlying microstructural characteristics of the neural tissues. It has shown promising results in studies on changes in gray matter and mild traumatic brain injury where DTI is often found to be inadequate. The DKI dataset, which has high-fidelity spatio-angular fields, is difficult to visualize. Glyph-based visualization techniques are commonly used for visualization of DTI datasets; however, due to the rapid changes in orientation, lighting, and occlusion, visually analyzing the much more higher fidelity DKI data is a challenge. In this paper, we provide a systematic way to manage, analyze, and visualize high-fidelity spatio-angular fields from DKI datasets, by using spherical harmonics lighting functions to facilitate insights into the brain microstructure.

Index Terms—Diffusion Kurtosis Imaging, Diffusion Tensor Imaging, Spatio-Angular Fields, Spherical Harmonics Fields, Tensor Fields

1 Introduction

Spatio-angular fields are defined by multiple (angular) vector fields defined over a shared 3D space. These fields are commonly used in physics and chemistry when analyzing gravity, geomagnetism, seismology, electric fields, and electron distributions around atoms. In radiology, the diffusion patterns measured by magnetic resonance imaging (MRI) are also expressed in spatio-angular fields. Although commonly encountered, outside of glyph representations, the visualization of spatio-angular fields has been barely explored in the visualization community.

MRI is a non-invasive tool that uses powerful magnetic fields to image biological tissues. Using MRI, one can detect the pattern of the diffusion of water movement using diffusion tensor imaging (DTI). DTI is effective in measuring the dominant direction of water diffusion in tissues and is widely used in studying white matter tracts in the brain [1, 16, 42]. However, traditional DTI is limited because the tensor estimation is based on the assumption that water diffusion patterns follow a Gaussian distribution. To measure the degree of the diffusional non-Gaussianity of water molecules in biological tissues, Jensen and Helpern [14] introduced diffusion kurtosis imaging (DKI). DKI has gained popularity as a valuable imaging technique to probe tissue microstructure, not only in white matter, but also in gray matter and in tumors, where diffusion is mostly isotropic and conventional DTI techniques lack sensitivity. DKI has shown great potential in many clinical applications, including tumor grading [33], neuro-degenerative diseases [7], traumatic brain injury [8, 51] and stroke [4]. In DKI, a kurtosis tensor is computed for each imaged voxel, which collectively defines a spatio-angular field.

The high-fidelity spatio-angular fields present in DKI are challenging to visualize. In these datasets, the angular vector multi-field at each voxel can be represented using a unique shape defined by its directional data. The shape of the spatio-angular field at each voxel is highly irregular in DKI because the fourth-order kurtosis tensor represents a more complex structure compared to the second-order diffusion tensor used in DTI. Statistical summarization of the per-voxel shape of the spatio-angular datasets (using super-quadrics, for instance) is a typical approach used for DTI datasets that might overlook important subtle details if used in DKI. Using glyphs for visualization is another common approach used in DTI and other imaging techniques [6, 32, 38, 49]; however, because of the high variation of spatio-angular fields in DKI, it is difficult to compare the per-voxel

- *Sujal Bista is with the University of Maryland at College Park, E-mail: sujal@cs.umd.edu*
- *Jiachen Zhuo is with the University of Maryland School of Medicine at Baltimore, E-mail: jzhuo@umm.edu*
- *Rao P. Gullapalli is with the University of Maryland School of Medicine at Baltimore, E-mail: rgullapalli@umm.edu*
- *Amitabh Varshney is with the University of Maryland at College Park, E-mail: varshney@cs.umd.edu*

Manuscript received 31 March 2014; accepted 7 July 2014; posted online 23 October 2014; mailed on 14 October 2014.
For information on obtaining reprints of this article, please send email to: tvcg@computer.org.

vector multi-fields due to occlusion, lighting, glyph density, and orientation. As the number of glyphs increases, the cost of rendering also increases; furthermore, the high visual density of glyphs makes them visually challenging to study. The highly irregular nature of these shapes limits the information conveyed by visualization if simplified glyphs are used.

To overcome these challenges, we propose the use of spherical harmonics lighting to visualize spatio-angular fields. We approximate spatio-angular fields using spherical harmonics basis functions. Then, using several spherical harmonics lighting functions, we illuminate the spatio-angular fields, expressing the underlying structure. This gives users an interactive way to visually explore and analyze any spatio-angular field. In this paper, we provide a systematic way to manage, analyze, and visualize spatio-angular fields (such as the shape of diffusion and kurtosis tensors used in DKI datasets) to facilitate insights into the micro-structural properties of the imaged volume. Our contributions are:

1. We use spherical harmonics lighting functions to allow researchers to explore, visualize, and analyze the subtle changes in the high-fidelity spatio-angular fields.
2. We incorporate 3D volume rendering by mapping spherical harmonics light integration of the spatio-angular field into the color and opacity to visualize structural properties present in these datasets.
3. We provide examples of case studies in traumatic brain injuries and cancer, where we apply our method to study the shape of diffusion and kurtosis tensors.

2 Related Work

Numerous studies and literature reviews have been conducted on how 3D structures (glyphs) are used to study, analyze, and segment tissues using various types of MRI.

Kindlmann [21] and Ennis *et al.* [6] used superquadric glyphs to visualize the tensor field and applied it on DTI datasets. These perceptually-motivated shapes greatly enhance the comprehensibility of the DTI microstructure. However, when the structure of the spatio-angular fields is too complex to be represented by superquadrics (as in DKI datasets), the effectiveness of these glyphs is limited.

Prckovska *et al.* [32] introduced a hybrid approach to visualize the structure of diffusion. They performed semi-automatic human-assisted classification of diffusion structures to separate different diffusion models, such as isotropic gray, anisotropic Gaussian, and non-Gaussian areas. Then, based on the classification, they used ellipsoids to display a simple diffusion shape and ray-traced spherical harmonics glyphs to highlight the complex structures.

Almsick *et al.* [49] presented a ray-casting-based approach to display a large number of spherical harmonic glyphs that are used to visualize high angular resolution diffusion imaging data. Their hybrid CPU- and GPU- based approach was able to interactively display large number of glyphs at interactive frame rates.

Similar glyph-based methods have been used by Lu *et al.* [28] and Lazar *et al.* [24] to visualize DKI. Lu *et al.* [28] used spherical harmonics basis to analyze the DKI dataset. They performed harmonic analysis of the first three bands and used coefficient summation to describe the rotationally invariant property of each band. Then they segmented white matter, gray matter, and fiber crossings. In their paper, they used glyph and image-based visualizations to study the DKI dataset. Lazar *et al.* [24] presented equations to approximate the orientation distribution function from DKI. For visualization, they also used glyphs. Both of these studies were focused on DKI analysis. Our paper is focused more on the visualization aspects, and we use a DKI dataset to visualize the diffusion kurtosis tensor. Our tool is also flexible in that it can incorporate the orientation distribution function presented by Lazar *et al.* [24].

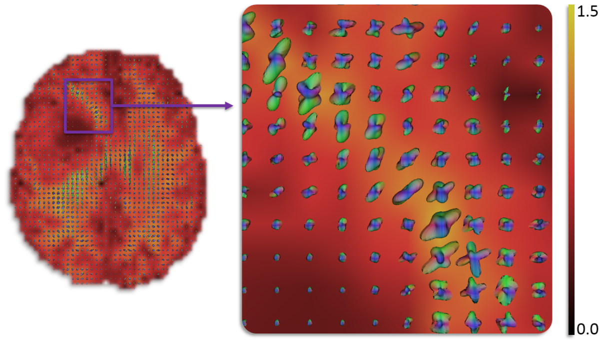

Fig. 2. Visualization of a DKI spatio-angular fields using traditional glyphs. This rendering is compute-intensive and due to occlusion, the density of glyphs, a difference in orientation, changes in lighting, and surface irregularity of the glyphs, the resulting visualization is cluttered and difficult to comprehend. Comprehension becomes an even bigger challenge when multiple planes must be shown.

Using glyphs with a reference image in the background has often been successfully used to visualize spatio-angular fields [6, 9, 32, 37, 38, 39, 49] such as DTI. However, for irregular and complicated shapes present in DKI, these glyphs demand a lot more computational power to render and are difficult to visually study. This is because 1) part of the glyphs are always occluded, 2) the density of the glyphs shown in the screen can be very high and will require the proper management of glyph size and zoom level, 3) there are changes in orientation and lighting between neighboring glyphs, 4) and the surface of the spatio-angular field can be highly irregular. When multiple planes must be shown, which is often the case in volumetric datasets, the visualization can become very cluttered. Saliency-based optimizations [18, 26] and local lighting [25] can be applied to glyph visualization to improve comprehensibility. However these techniques do not address the key drawbacks associated with glyph-based visualization. Although the proposed method supports glyph-based visualization (Figure 2), we primarily provide viewing mechanisms based on spherical harmonics lighting.

For second order tensors present in DTI, Kindlmann and Weinstein [19] and Kindlmann *et al.* [20] have used barycentric mapping, hue-ball, and lit-tensor methods to visualize the direction of anisotropy, the type of anisotropy, and the shape of the diffusion tensor matrix [19, 20]. Using these methods they compute color and opacity for volume rendering. Their approach cannot be directly applied to visualize high-order tensors like those in DKI because they have highly irregular and complicated shapes. In our work, we use spherical-harmonics lighting functions that allows us to visualize high-order tensors.

Schussman and Ma [41] used anisotropic volume rendering to visualize dense lines. By taking viewpoint into consideration, they accumulated the average color and opacity contribution for every voxel and stored its spherical harmonics representation. While rendering, they converted anisotropic representation into standard voxels by evaluating spherical harmonics approximation. In our work, we use various lighting functions (which can be complicated shapes themselves) and their combinations to study the shape of spatio-angular fields. These lighting functions allow investigators to study irregular fields, such as DKI datasets, in a variety of different ways.

Volume rendering is widely used to visualize MRI datasets. Extensive work has been done to improve visualization by using advanced shading techniques, multiple depth cues, transfer functions, and global illumination [5, 10, 11, 22, 23, 27, 29, 35, 46, 47, 50]. Transfer function that maps size of features to color and opacity has been shown by Correa and Ma [5] to greatly improve classification and visualization. For multiple lighting designs in volume rendering, Tao *et al.* [46] used an automatic lighting design based on the structure of the scene by measuring the structural changes in the images. In recent work by Zhang and Ma [50], a three point lighting system was used to enhance the depth and the shape of the volume. An interesting alternative to direct volume rendering of diffusion MRI datasets is to visualize their tensor topology [36, 40, 48]. This line of research extends the basic concepts of flow topology, such as critical points, lines, basins, and faces, to tensor fields with suitable interpretations in terms of features in the brain anatomy. These studies on volume rendering contain remarkable ways to enhance the visualization of the scalar- and tensor-fields being displayed. Our work focuses on representing the structure of tensors in the spatio-angular field and, with the aid of spherical harmonics lighting functions, visualizing them through multiple rendering techniques, including volume rendering.

3 Overview

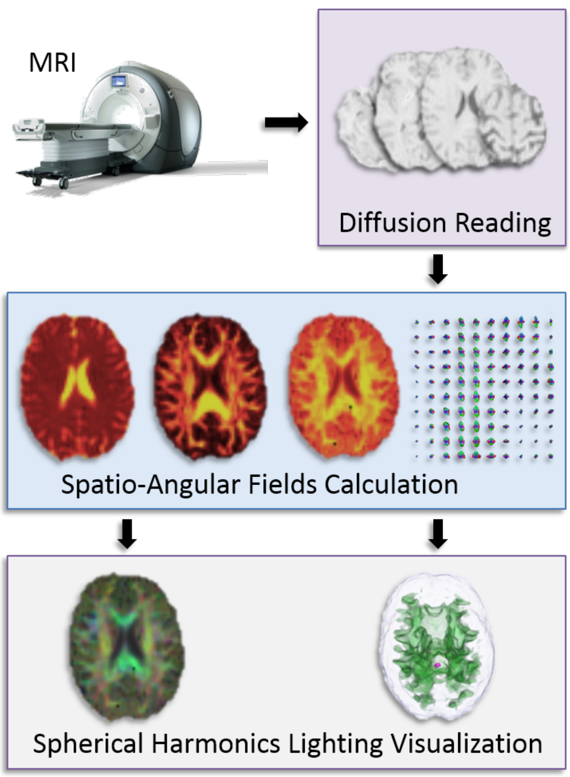

Fig. 3. Overview of the proposed method. First, a large number of diffusion readings are recorded using MRI. Second, domain-specific processing is performed to compute values such as mean diffusion, fractional anisotropy, mean kurtosis, and diffusion/kurtosis tensors. Then, depending on the task and the complexity of the field, we select either a single or multiple spherical harmonics lighting functions. Finally, by combining the dynamic spherical harmonics lighting functions and the input spatio-angular field, the dataset is rendered. The output is either a planar-rendered image, a volume-rendered image, or both.

The proposed method takes spatio-angular fields as an input and converts them into spherical harmonics fields using spherical harmonics basis functions. Depending on the task and the complexity of the field, we either choose to configure a single or multiple spherical harmonics lighting functions. Finally, by combining classified segments, the dynamic spherical harmonics lighting functions, and the input spatio-angular field, we render the dataset. We provide two modes to view the final output using either planar or volume rendering. An overview of the system is shown in Figure 3.

4 Background

4.1 Diffusion Tensor Imaging

DTI considers the diffusion process to be Gaussian. For each gradient direction, the diffusion-weighted signal is approximated by the Taylor series expansion [16] given by the equation

$$ln\left[S\left(g,b\right)\right] = ln\left[S_0\right] - bD_{app}\left(g\right) + O\left(b^2\right),$$

$$D_{app}\left(g\right) = \sum_{i=1}^{3}\sum_{j=1}^{3} g_i g_j D_{ij},$$

where g is a diffusion gradient, b is the MRI acquisition parameter b-value expressed in s/mm^2, S_0 is the signal without diffusion weighting, D_{ij} is the element of the diffusion tensor, and D_{app} is the apparent diffusion coefficient. The diffusion tensor is a second order symmetric tensor with six independent elements. In DTI, the diffusion tensor is calculated for each voxel. The direction of the dominant eigenvector of the diffusion tensor is often used in fiber tracking.

4.2 Diffusion Kurtosis Imaging

The non-Gaussian property of water diffusion is measured in DKI. There are limitations in the traditional DTI technique because the tensor estimation is based on the assumption that water diffusion patterns follow a Gaussian distribution. While this may be true over larger diffusion time scales, it is less effective when the diffusion time is shortened, or in other words, when exploring even shorter diffusion distances of the water molecule. The measurement of diffusion over shorter time periods sensitizes the technique to the local diffusion heterogeneity reflective of the tissue micro-environment. This diffusion heterogeneity tends to make the probability distribution function for water diffusion non-Gaussian, suggesting that the normal way of obtaining the diffusion tensor which assumes Gaussian distribution, is no longer valid [15]. To measure the degree of the diffusional non-Gaussianity of water molecules in biological tissues, Jensen and Helpern [14] introduced DKI. Data acquisition needs are much larger in DKI compared to acquisition in DTI. The kurtosis tensor is often computed using data from 30 diffusional directions using at least two non-zero diffusion sensitivities. Common b-values used in DKI acquisition are 0, 1000, and $2000s/mm^2$, and the scan time can be as long as 10min. Other forms of higher order diffusion-weighted imaging techniques, such as high angular resolution diffusion imaging or diffusion spectrum imaging, use a much higher number of diffusional direction and b-values and, hence, are less clinically practical as they take a considerably longer time to scan. To measure the non-Gaussian property of the water diffusion, the Taylor series equation is further expanded [14, 15]. From the diffusional measurements in DKI, a fourth order diffusion kurtosis tensor is calculated by using the equation described by Jensen and Halpern [15].

$$ln\left[S\left(g,b\right)\right] = ln\left[S_0\right] - bD_{app}\left(g\right) + \frac{1}{6}b^2 D_{app}\left(g\right)^2 K_{app}\left(g\right) + O\left(b^3\right),$$

$$K_{app}\left(g\right) = \frac{1}{D_{app}\left(g\right)^2}\sum_{i=1}^{3}\sum_{j=1}^{3}\sum_{k=1}^{3}\sum_{l=1}^{3} g_i g_j g_k g_l K_{ijkl},$$

$$K_{ijkl} = MD^2 W_{ijkl},$$

where MD is the mean diffusivity, K_{app} is the apparent kurtosis, and W_{ijkl} is the element of kurtosis tensor. The kurtosis tensor is a symmetric fourth order tensor with 15 independent elements. In full form, the signal in each gradient direction is described by

$$ln\left[S\left(g,b\right)\right] = ln\left[S_0\right] - b\sum_{i=1}^{3}\sum_{j=1}^{3} g_i g_j D_{ij} + \frac{1}{6}b^2 \sum_{i=1}^{3}\sum_{j=1}^{3}\sum_{k=1}^{3}\sum_{l=1}^{3} g_i g_j g_k g_l K_{ijkl},$$

4.3 Spherical Harmonics

In our method, visualization of the spatio-angular fields is performed by using the spherical harmonics lighting functions. Spherical harmonics are basis functions that are used to represent and reconstruct any function on the surface of a unit sphere. Fourier functions are defined on the circle, whereas spherical harmonics are defined over the surface of a sphere [30]. In visualization and graphics, spherical harmonics are used for lighting scenes with low frequency lights. It is a fast technique often used to approximate a computationally complex physical process, such as subsurface scattering and global illumination [3, 17, 35, 43, 44, 50].

Spherical harmonics are ortho-normal functions defined by

$$Y_l^m(\theta,\phi) = (-1)^m \sqrt{\frac{2l+1}{4\pi}\frac{(l-m)!}{(l+m)!}} P_l^m(\cos\theta) e^{im\phi},$$

where l is the band index, m is the order, P_l^m is an associated Legendre polynomial, and (θ,ϕ) is the representation of the direction vector in the spherical coordinate. Since the values used to define spatio-angular fields are positive and real, we use real-valued spherical harmonics.

To convert the function $f(\theta,\phi)$ into spherical harmonics basis, spherical harmonics coefficients a_l^m are approximated using the equation

$$a_l^m = \int_s f(\theta,\phi) Y_l^m(\theta,\phi) ds,$$

Once the coefficients are computed, the function $f(\theta,\phi)$ can be approximated by using the equation

$$f(\theta,\phi) = \sum_{l=0}^{\infty} \sum_{m=-l}^{l} a_l^m Y_l^m(\theta,\phi),$$

One key advantage of spherical harmonics representation is that integrating two functions over the sphere can be approximated easily by performing a dot product of their spherical harmonics coefficients [2, 17].

$$\int U(s) \times V(s) ds = \sum_{i=0}^{l^2} u_i(s) \times v_i(s),$$

where U and V are two functions defined on the surface of a sphere, and $u(s)$ and $v(s)$ are their spherical harmonics coefficients.

5 Diffusion Kurtosis Imaging Data

Imaging was performed using a 3T Siemens Tim Trio Scanner (Siemens Medical Solutions; Erlangen, Germany). Diffusion weighted images were obtained with $b = 1000, 2000 s/mm^2$ at 30 directions, together with 4 b_0 images, in-plane resolution $= 2.7mm^2$, echo time/time repetition $= 101ms/6000ms$ at a slice thickness of $2.7mm$ with two averages. DKI reconstruction was then carried out on each voxel using a MATLAB program as described by Zhuo *et al.* [51].

After diffusion and kurtosis tensors are computed, we represent the shape of these tensors by using spherical harmonics approximation. We use D_{app} and K_{app} to find the shape represented by the diffusion and the kurtosis tensor, respectively. The shape is then transformed into a spherical harmonics basis by computing spherical harmonics coefficients a_l^m to approximate the shapes of both the diffusion and kurtosis tensor. The shape of the diffusion tensor is simpler than the kurtosis tensor. For kurtosis, we use up to five bands to represent the shape; however, as described by Lu *et al.* [28], bands 2 and 4 do not contain any information, as the structure of the tensors are symmetric. Using a greater number of bands (> 5) is considered less beneficial, as high frequency data in both tensors contains more noise, as discussed in [28]. Once data is transformed to spherical harmonics basis for each shape in a voxel, we have up to 15 spherical harmonics coefficients (there are 25 coefficients in total, but bands 2 and 4 are not used). These coefficients capture the shape, magnitude, and direction of the tensors. This approximation, using 15 spherical harmonics coefficients, is used for exploration and visualization.

6 Approach

Our method can be divided into two major steps: lighting function selection and visualization. Details of each step are described in the following sections.

6.1 Lighting

The key idea of our approach is to use the spherical harmonics lighting functions to visualize the spatio-angular fields. We define spherical harmonics lighting functions as basic shapes expressed in spherical harmonics basis that define different query functions researchers are interested in. The shape, size, orientation, and combination of the lighting functions defines the output of the visualization. By making changes in these attributes, one can study a variety of characteristics expressed in the spherical harmonics fields that may be representative of the local tissue microstructure.

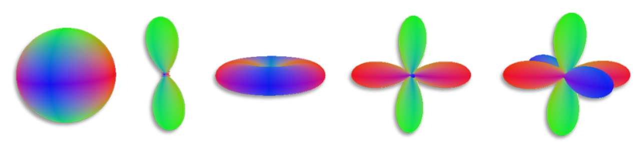

Fig. 4. Representative lighting functions used to analyze spatio-angular fields. The shape and the size of these spherical harmonics lighting functions can be altered to analyze different properties. The first function shown above, which is spherical, is used to compute the average value. The next four functions are used to compute single and multiple directional properties of the spatio-angular field. These lighting functions can be rotated or combined with other functions as desired.

Lighting spatio-angular fields: Spherical harmonics lighting is used to explore the directional strength of the spatio-angular field. In Section 4.3, we explained how spherical harmonics is used for lighting in visualization and graphics. We extend the application of spherical harmonics to visualize spatio-angular fields. Having expressed lighting functions and the volume field in spherical harmonics basis, we compute the light response value R for each light p using the equation $R_p = k \times \sum_{i=0}^{l^2} u_i(s) * v_i(s)$, where $u(s)$ and $v(s)$ are their spherical harmonics coefficients of the lighting function and a data point in the spatio-angular field, respectively. k is used to scale the light response value in order to map it to the visual range ($[0-1]$) used in rendering.

Shape and Size: The shape of a spherical harmonics lighting function is one of the main attributes that determines how a spatio-angular field is visualized. Some common shapes are spherical, directional lobe, cross-sectional lobes, and radial lobe, as shown in Figure 4. The shape can be roughly divided into two parts, the directional component and its angular strength. The directional component expresses the incident path of the light, which is used to explore the strength of the spatio-angular field in the given direction (in DKI dataset, the strength of the spatio-angular field is the apparent kurtosis value). The angular strength corresponds to the area of the light. The range of angular strength is $0-360$ degrees. When the angular strength of the spherical harmonics lighting function is set to maximum, a spherical shape is formed. Lighting the spatio-angular field at this setting will give the mean strength of the field in all directions shown in Figure 5(a). By using a small value (for example, 30 degrees) for angular strength, we are able to study the strength of the spatio-angular field in any given direction shown in Figure 5(b). Spherical harmonics lighting with a radial-shaped lobe has a very useful property. It can be used to find

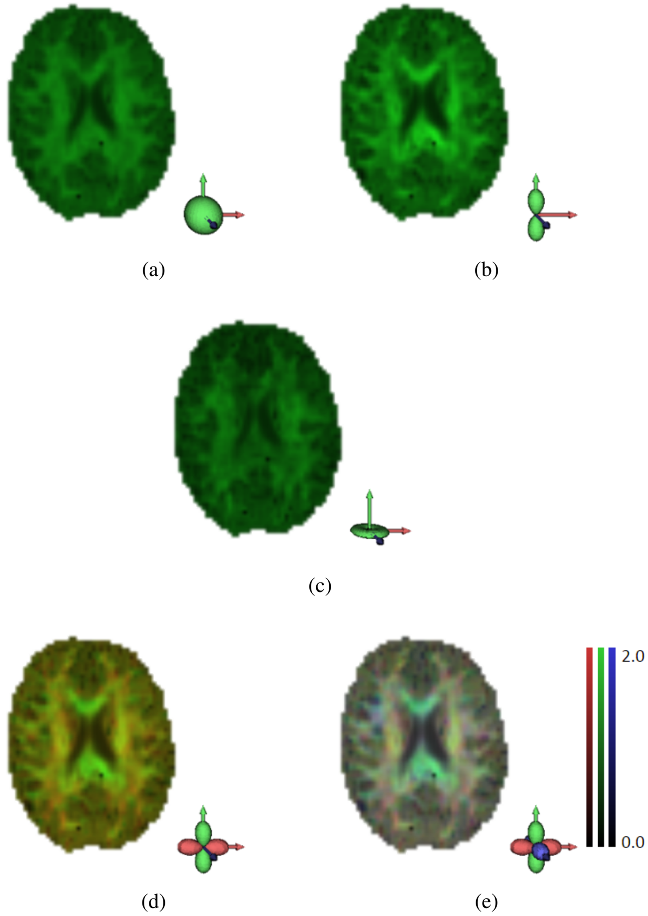

Fig. 5. The effect of using different lighting functions. We use various lighting functions on the same MRI and show different views of the structural properties of the underlying spatio-angular fields. The orientation of these lighting functions can be adjusted to investigate directional changes in the diffusion profile. In Figure 5(a), we use a spherical lighting function, which provides the mean strength of the field in all directions. In Figure 5(b), we use the directional lobe aligned with the y-axis to show the strength of the spatio-angular field in the y direction. Similarly, in Figure 5(c), we use the radial lobe. In Figure 5(d) and Figure 5(e), we use multiple lighting functions with different colors mapped to each axis. Color bars with a numerical range are shown on the side of the image to illustrate the color scale used.

the strength of values orthogonal to any given direction. This is beneficial in studying kurtosis tensor, as kurtosis values are very high in the direction orthogonal to the principle diffusion direction as shown in Figure 5(c). Taken together, the variations of the lighting functions provide a means to probe the tissue microstructure. Most normal tissues in the brain are generally characterized as gray matter, white matter, and cerebrospinal fluid. The spherical harmonics lighting allows researchers to further probe local tissue microstructure. An injured region of the brain may result in spatio-angular field of several shapes and sizes. In such cases the heterogeneity shown by the spherical harmonics lighting method can highlight of the local changes in the tissue microenvironment compared to a similar tissue in another region of the brain. In Figure 5, we show effect of using different lighting functions. The shape of the spatio-angular fields and the properties of the lighting function create different light response values, as shown in Figure 6.

All of the lighting functions are expressed in spherical harmonics basis. For directional and radial lights, we define functions (F_{dir} and F_{rad}) on the surface of the sphere given by equation

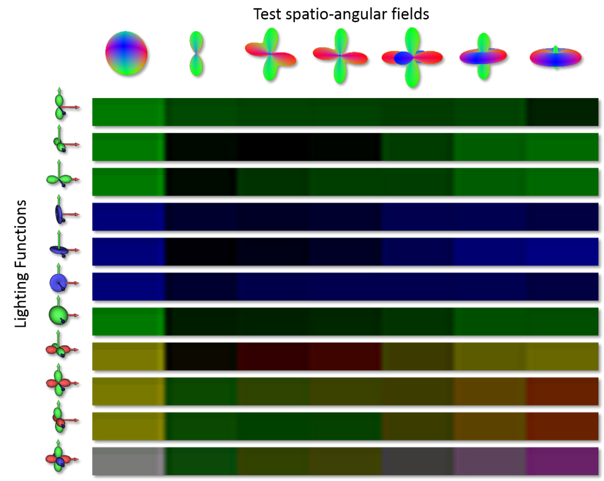

Fig. 6. The color table shows the light response values arising from the application of representative lighting functions (left) on various spatio-angular fields (top).

$$F_{dir}(g) = \begin{cases} 1 & \text{if } (g \cdot g_{light}) > cos(a * 0.5), \\ 0 & \text{otherwise.} \end{cases}$$

$$a_{rad} = \begin{cases} 90 - a * 0.5 & \text{if } (90 - a * 0.5) > 0, \\ 0 & \text{otherwise.} \end{cases}$$

$$F_{rad}(g) = \begin{cases} 1 & \text{if } ((g \cdot g_{light}) < cos(a_{rad}), \\ 0 & \text{otherwise.} \end{cases}$$

where a is angular strength, g_{light} is the direction of the light, g is unit direction. For symmetric lighting function, absolute value of the dot product is taken. These are the various lighting functions used for DKI datasets. Depending on the dataset, different lighting functions with different properties can be added.

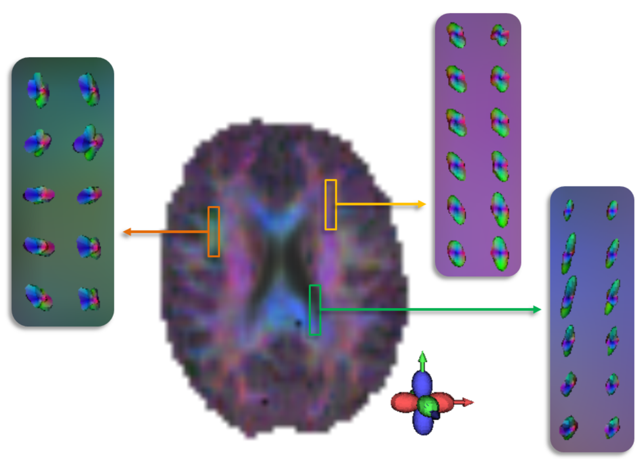

Fig. 7. Spherical harmonics lighting allows users to easily study the shape of spatio-angular fields and get an appreciation of the local water diffusion environment. The spherical harmonics lighting function captures information about the shape of spatio-angular fields. Here we are using three directional spherical harmonics lighting functions and displaying the relation between them and the tensors at each voxel. We use red, green, and blue colors for each spherical harmonics lighting function. The sub-images show the individual shapes of the kurtosis tensors. The variation in shape is captured by a spherical harmonics lighting function and can be observed by the change in the color.

Global Orientation: The direction of the spherical harmonics lighting function allows us to gauge the strength of a spatio-angular field in any desired direction. One can dynamically rotate the spherical harmonics lighting function to examine how the field is changing or how heterogeneous the environment is to water diffusion. By combining multiple lighting directions, studying multiple aggregated directions at any given time is possible. This is often desired when the individual shapes in the spatio-angular fields have some known relation, such as symmetry. The adjustable lighting orientation will also allow researchers to probe the directional changes of the diffusion profile, which can be especially useful when studying complex tissue microstructure (e.g. regions around lesions).

Local Orientation: Information about local coherences can be utilized by spherical harmonics lighting to provide visualization of local properties. We applied this local adjustment to both DTI and DKI datasets. The diffusion values are dominant in the principal diffusion direction for each voxel and can be connected together to form a path if the fractional anisotropy (FA) value is also high. When the direction of the lighting function is aligned with the principal diffusion direction, diffusion and kurtosis values along the path can be visualized. In other words, it is quite possible to follow a fiber tract. For this visualization, we align the z-axis of the spherical harmonics lighting function with the first eigenvector of the diffusion tensor for every voxel, as shown in Figure 8. This will cause the direction of the light to be different for every voxel that is along the local coherences between the voxels. By interacting with the application, users are able to determine how the values change within the path. Figure 8 shows this application on the kurtosis datasets. However, aligning the direction of the light based on the principal diffusion direction of DTI has a drawback; in areas that have fiber crossings, all three eigenvalues of the diffusion tensor can be similar. This can cause the principal diffusion direction to change from one voxel to another. This limitation can be addressed by using an improved fiber tracking algorithm that takes into consideration noise and distortion artifacts [12, 13, 31, 34], improved fiber crossing detection algorithm [45], and by using lights with multiple lobes for those regions.

Multiple Lighting: Multiple simple shapes can be combined to create a complex lighting function. Multiple lighting functions allow the researchers to study the strength of a spatio-angular field on different shapes separately. This is slightly different from having multiple directional lobes in one lighting function. Using multiple lighting functions results in a separate light response value R_p for each light, whereas using one lighting function with multiple directional lobes provides an aggregated view of the tissue microstructure. The lighting combination has a large number of applications. For example, when we applied three orthogonal lighting directions to the DKI dataset, we were able to determine both the magnitude and directional variation present in the spatio-angular field. The result is shown in Figure 7. Here we used red, green, and blue colors for each spherical harmonics lighting function. The right sub-images show the individual shapes of the kurtosis tensor. Notice how the change in shape can be observed by the change in the color. In Figure 9, we demonstrate the contribution of individual lights in the brain of a patient who suffered a traumatic brain injury, along with the aggregated final image.

The principal diffusion direction points to the direction of the white matter axons. Probing into the directional kurtosis tensor in this direction offers information about the direction of the diffusion restriction. Probing along the two minor diffusion directions will also provide complementary information regarding diffusion. Hence, the combination of the two can potentially provide powerful information such as the general status of the axons and the degree of myelination or loss in myelination of the axons. Such information can provide extremely useful insights not only regarding the status of the tissue microenvironment, but also can be useful when evaluating the therapeutic efficacy of new drugs.

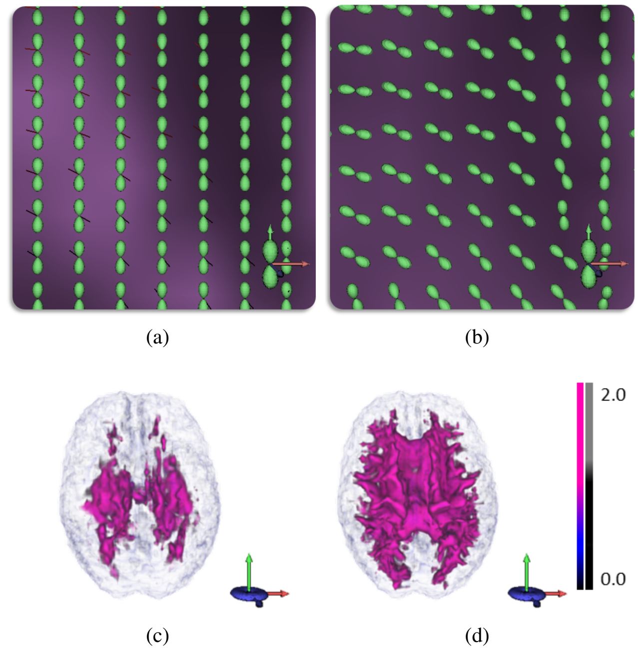

Fig. 8. The orientation of the lighting function can be global or local. Figure 8(a) shows the global orientation, where each data point is illuminated with the lighting function (show in green glyph) oriented consistently across the entire dataset. Figure 8(b) shows the local orientation, where each data point is lit with the lighting function locally oriented towards the principal diffusion direction of the diffusion tensor. Often, there is a local coherence between neighboring data points. For example, a fiber tract might go through them. To visualize the properties along a path, a directional spherical harmonics light can be independently aligned with the desired direction for each data point. For Figure 8(c), the global lighting direction is used. For Figure 8(d), we align the light along the principal diffusion direction for each data point and display how the kurtosis values change. Kurtosis values are dominant in the direction orthogonal to the principal diffusion direction of each data point. Both Figure 8(c) and Figure 8(d) are rendered by using method described in Section 6.2.

6.2 Visualization and Interaction

We use two methods to visualize the spatio-angular fields.

Planar Visualization: In this mode of visualization, only one plane of the spatio-angular field is shown at a time. For each data point in the plane, we apply the spherical harmonics lighting by computing the light response value R_p and then mapping it to the color space using a transfer function. After that, the color contribution of all the lights is integrated together to compute the final color C of the voxel using the equation $C = \sum_i T_i(R_i)$, where T is the transfer function that maps light response value to a color value. Examples of this mode of visualization are shown in Figure 7 and Figure 9. It incorporates the shape information of each visible data point in spatio-angular fields through changes in color and intensity.

Volume Visualization: In this mode of visualization, we incorporate our method with a widely used volume rendering technique to show the entire dataset. Volume visualization allows researchers to analyze and visualize scalar fields with multiple layers at the same time, which has the potential to provide a complete picture of the dataset.

Dynamic light functions are used to map spatio-angular data to the surface of the volume. Typical volume rendering is done with scalar-field data. To perform volume visualization of a spatio-angular field, we first apply spherical harmonics lighting to each data point as we described it for the planar visualization mode. Depending on the number of lights used, we may compute multiple light response values R_i. These values can be used to directly perform the transfer func-

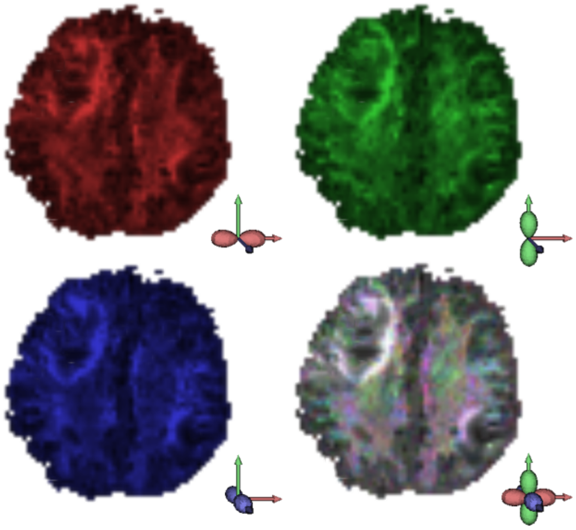

Fig. 9. By combining multiple directional spherical harmonics lighting functions, we can produce an overview of the spatio-angular field. In this image, we use kurtosis data to summarize the injured region. The first three images (red, green, and blue) reveal how the shape varies in the $x-$, $y-$, and $z-$axes, respectively. The final image is the summation. Notice how structural changes in the spherical harmonics lighting function capture different properties of the imaged tissue.

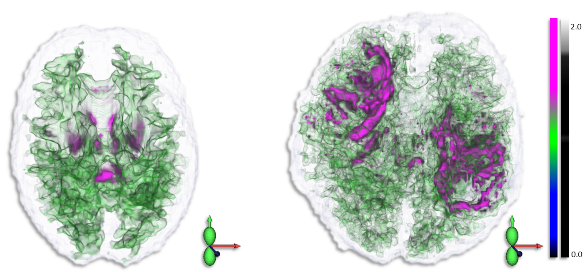

(a) Normal Subject (b) Injured Patient

Fig. 10. The directional kurtosis value of a normal subject and an injured patient using the spherical harmonics lighting tool. The coloring transforms from blue to green to red to denote the increasing value of kurtosis. In the injured patient, the region around the injury (seen in the red box) has a very high kurtosis value. By rotating the light, the response values of each data point are changed. When combined with a transfer function that has variations in opacity, users can study the magnitude and directional changes at the same time.

tion lookup for each light separately. However, to reduce texture lookups, we use the mean light response for performing transfer function lookup. The transfer function lookup obtains information about opacity and color value. When the lighting function or its orientation is changed, the light response value also changes. This results in a different lookup of the transfer function which causes the iso-value-light-response-surface of the volume to change. We thus map the structure of the spatio-angular field to a rendered surface. This can be seen in Figure 8(c) and Figure 8(d) where we use global and local lighting orientation, respectively, to display the underlying spatio-angular field structure.

The opacity of each voxel is directly determined by the result of the transfer function lookup. However, to compute the color value, we have two options. We can either use the mean light response to do a color lookup from the transfer function or we can treat the lights as having different colors. We can further improve the visualization by incorporating monocular depth cues, such as shadows, ambient occlusion, and edge enhancement. In some cases visualization of dynamic volumes can be greatly enhanced by coherent modification of a local transfer function, as suggested by Tikhonova et al. [47]. However in our case, since the range of kurtosis values do not vary dramatically we have found that having a single (global) transfer function suffices.

In Figure 10, we show the volume rendering of both a normal subject and an injured patient. Here, kurtosis values are differentiated based on color. The regions with injury in the volume rendered images are clearly depicted and represent the extreme kurtosis values, and the location of these high kurtosis values are consistent with the coup and contra-coup injury pattern typically seen in traumatic brain injury patients.

Interaction: For user interaction, we use mouse-based input and screen-based sliders. Using these input widgets, users can change the direction, size, and shape of the lighting function.

7 Case Study

Clinicians use several different images for the diagnosis of injuries and diseases of the brain. Mean diffusion, fractional anisotropy, and principal diffusion directional color maps are used to study the Gaussian behavior of the diffusion with DTI. With DKI, an additional mean kurtosis map is used. The kurtosis tensor is a complex structure. Our tool allows researchers to study such complex shapes easily. We will now examine several case studies.

7.1 Case Study I

In Figure 11, we visually compare these different maps with the image generated using our tool. We have demonstrated that the region around the injury, which has very high kurtosis values can be visualized easily (Figure 11(e)). Furthermore, images depicting the structural information can also be generated using our tool (Figure 11(e) and Figure 11(f)). By interacting with the lighting functions, users can appreciate the local micro-structural information in any direction.

7.2 Case Study II

Another injury case is shown in Figure 12, where the injury is subtler, with no obvious lesions in the patient. However, the patient has sustained post-concussive symptoms, declined cognitive function, and brain atrophy. Using our tool, we examine the shape of the kurtosis tensor that is orthogonal to the principal diffusion direction of each data point. It is well-known that kurtosis is higher in these areas. In Figure 12, we show the difference observed in kurtosis values with the loss of white matter integrity, which is inline with the patient's clinical status.

7.3 Case Study III

In the injury case shown in Figure 13, the patient has sustained frontal lobe damage. The patient showed impressive recovery at a one month follow-up after the injury. The rendering of the kurtosis tensor with local spherical harmonics lighting showed improvement of the frontal lobe white matter structure, which was otherwise missed by the diffusion tensor.

7.4 Case Study IV

In this case, we look into the MRI of a patient with a tumor. High kurtosis values are observed around the tumor region, which were not visible in mean diffusion, fractional anisotropy, or principal diffusion directional color map weighted by fractional anisotropy. With the use of spherical harmonics lighting, additional structural information can be seen, which is shown in Figure 14(d).

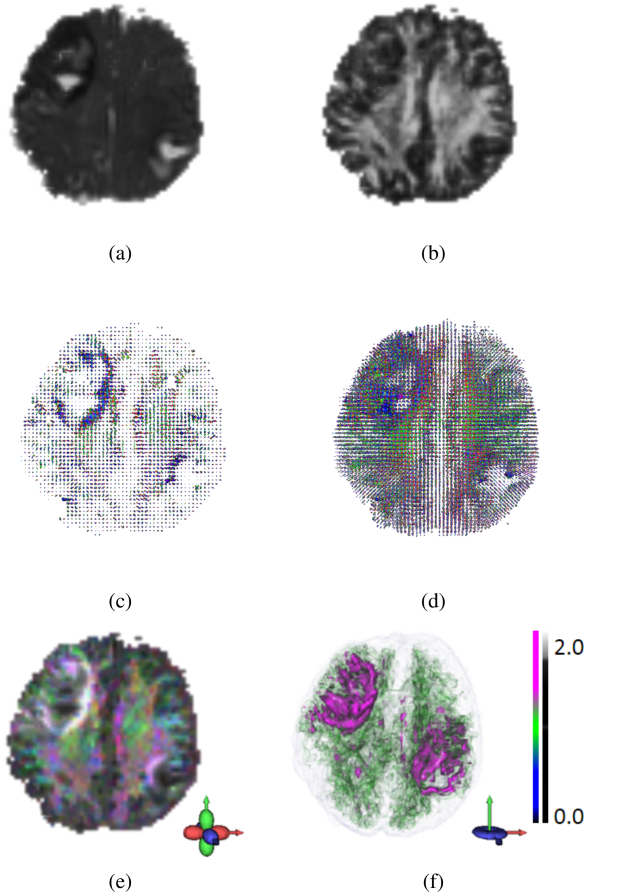

Fig. 11. We visually compare different color maps and data visualization methods, such as mean diffusion (Figure 11(a)), fractional anisotropy (Figure 11(b)), single-layer glyph visualization of DKI data (Figure 11(c)), and multiple-layer glyph visualization (using seven layers) of DKI data (Figure 11(d)). Kurtosis values are very high around the injury region and are vital to assess the extent of the injury. Also generated by our tool, Figure 11(e), incorporates structural information through the changes in color and intensity from the DKI data into the visualization. Figure 11(f), generated using local spherical harmonics lighting, shows the entire volume. Although glyphs (Figure 11(c) and Figure 11(d)) contain the complete spatio-angular data, occlusion and scaling makes comprehension difficult.

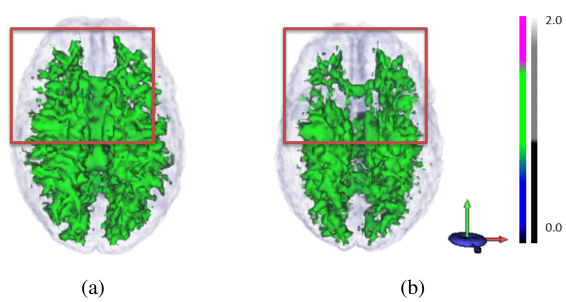

Fig. 12. We compare the MRI of a patient taken 10 days (left) and 6 months (right) after a traumatic brain injury. We use a radial spherical harmonics light to show the kurtosis value orthogonal to the principal diffusion direction of each data point. Despite a lack of anatomical changes in the patient, severe changes in kurtosis values, highlighted in the red box, are observed over time.

8 Evaluation

Two of the authors on this paper (Drs. Zhuo and Gullapalli) are acknowledged experts in medical research working with DKI. Their clinical expertise was key in evaluating our visual tool. After a brief tutorial, they used the tool on various datasets; they pointed out several useful features of our system. The planar visualization mode allows visualization of directional diffusion and kurtosis values along any arbitrary direction, a valuable tool when probing the directional profile of tissue microstructure in or around lesion areas. Our system also overlays diffusion and kurtosis glyphs for each voxel when a detailed view of tensors is needed for selected regions. Experts find our visualization method combined with existing glyph-based visualization useful. Furthermore, the software allows for easy toggling between various maps generated by different lighting functions with color coding, which eases the task of identifying abnormal tissue contrasts. In the volume visualization mode, spatio-angular data is mapped onto the surface of the volume using the transfer function. This allows users to find and highlight the rendered brain areas with abnormal diffusion values. They also found the adjustment of the transfer function to be straightforward and powerful when exploring the dataset in volume visualization mode. The main limitation of this visualization tool is a lack of a user-friendly graphic interface for ease of interaction. The current version of our system is mainly focused on visualization and a better user interface would be clearly desirable to enhance a broader usage of our work.

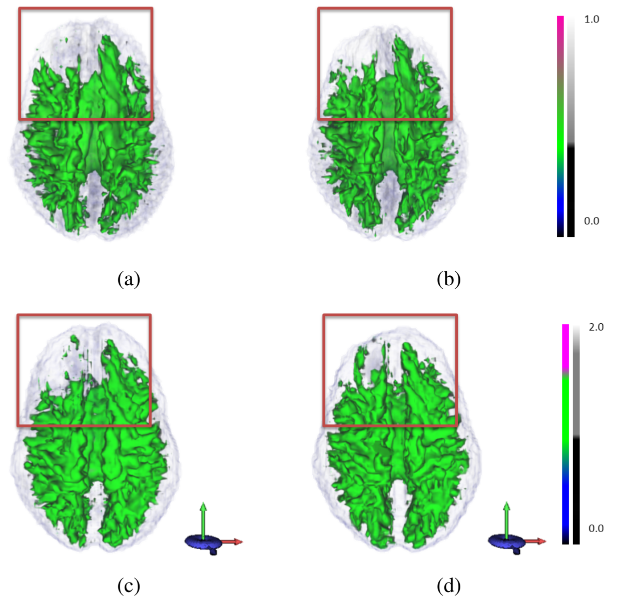

Fig. 13. We compare the MRI of a patient taken 8 days (Figure 13(a) and Figure 13(c)) and 1 month (Figure 13(b) and Figure 13(d)) after a traumatic brain injury. In Figure 13(a) and Figure 13(b), we show volumetric rendering using the traditional fractional anisotropy value, and in Figure 13(c) and Figure 13(d) we show volume visualization using local spherical harmonics lighting. The recovery of the patient can be better visualized using our approach in (d) than using the traditional fractional anisotropy in (b).

9 Discussion

Creating, visualizing, and interacting in our visual tool's planar visualization mode does not require any expertise. Both coloring and interaction are straight forward. However, volume visualization requires users to select transfer functions with color and opacity information. The output of visualization requires properly selecting such functions, which is typical for all volume rendering applications. Selecting opacity effectively also depends on the data being used. Since we are dealing with soft tissues, the intensity-gradient histogram does not have areas that can be easily segmented, as performed by [11]. To simplify this process, we create a transfer function, taking into account the distribution of diffusion and kurtosis values of well-known regions of the brain.

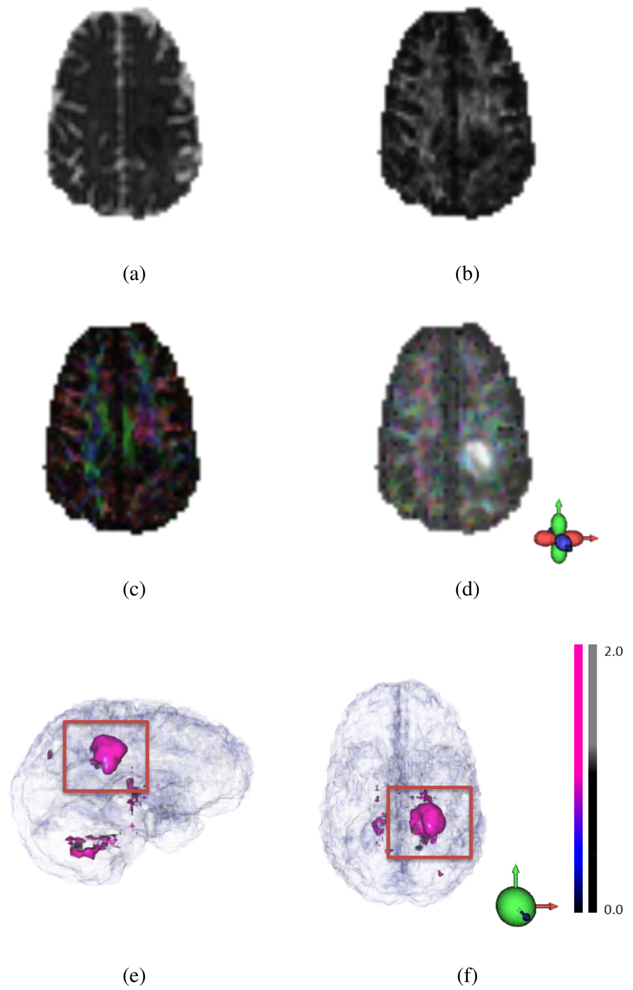

Fig. 14. Here we visually compare different color maps (such as mean diffusion, fractional anisotropy, principal diffusion directional color map weighted by fractional anisotropy, and mean kurtosis) with the image generated using our tool. Kurtosis is very high around the tumor, as seen in Figure 14(d), Figure 14(e), and Figure 14(f). With the use of spherical harmonics lighting additional structural information can be seen in Figure 14(d).

By using the lighting functions, the directional information of any complex shape can be observed. Key advantages of using the spherical harmonics lighting function include allowing us to a) analyze a spatio-angular field in any desired direction with any desired function, b) interactively explore the spherical harmonics field, c) easily compare values in any given direction without occlusion, scale, and density problems, which often occur when glyphs are used, d) effortlessly locate local changes, e) easily aligns in with the extensively researched direct volume rendering for visualization, and f) customize for various datasets with only minor changes.

In DTI, the direction of the principal diffusion in regions with high fractional anisotropy is very important. In a study by Schwartzmann *et al.* [42], the difference in principal diffusion direction between good and poor readers was observed. Kurtosis tensors are more complex than diffusion tensors. Directional information that can be shown easily through spherical harmonics lighting can be a vital tool for radiologists. As already illustrated in Lazar *et al.*'s paper [24], the shape of the kurtosis tensor provides information about crossing fibers within a voxel, which is not depicted by the diffusion tensor. In more complex tissue environments (e.g. surrounding lesions in the brain in Figure 10), the kurtosis tensor is able to depict a unique shape and, may be reflective of the direction of tissue scaring, while the diffusion tensor only indicates non-directional restriction (low fractional anisotropy and low mean diffusion). These unique shapes can be studied by using various spherical harmonics lighting functions.

Although multiple lighting functions can be used to summarize the spatio-angular field, spherical harmonics lighting is designed to be an interactive tool. Interaction (by rotating the lighting functions) is required to exploit full power of the spherical harmonics lighting, whereas glyph-based visualization can be static especially when the number of glyphs is low. Both of these methods can be used together as they complement each other.

10 Conclusions And Future Work

We have presented the use of spherical harmonics lighting to assist users in visually exploring and analyzing spatio-angular fields that are approximated by spherical harmonics basis functions. Our approach includes spherical harmonics based lighting and visualization. Our interactive approach allows researchers to easily visualize information about the shape, magnitude, and direction for each data point of a spatio-angular volume field. We have applied this method to state-of-the-art diffusion kurtosis imaging, which can assist in visualization of the brain's complex microstructure.

In the future, we hope to extend the utility of our tool to various disease processes involving the human brain to study inflammation and neurodegeneration. We also hope to explore other spherical basis functions, such as spherical wavelets.

Acknowledgments

We cordially thank Carlos Correa, Cheuk Yiu (Horace) Ip, Joseph JaJa, Gordon Kindlmann, Kwan-Liu Ma, and Raghu Machiraju, for their valuable feedback and suggestions on earlier versions of this paper. We are grateful to the anonymous reviewers whose constructive comments have greatly improved the presentation of our approach and results in this paper. We appreciate the support of the US Army grant W81XWH-12-1-0098, NSF grants 09-59979 and 14-29404, the State of Maryland's MPower initiative, and the NVIDIA CUDA Center of Excellence. Any opinions, findings, conclusions, or recommendations expressed in this article are those of the authors and do not necessarily reflect the views of the research sponsors.

References

[1] L. M. Baker, D. H. Laidlaw, T. E. Conturo, J. Hogan, Y. Zhao, X. Luo, S. Correia, R. Cabeen, E. M. Lane, J. M. Heaps, et al. White matter changes with age utilizing quantitative diffusion MRI. *Neurology*, pages 10–1212, 2014.

[2] B. Cabral, N. L. Max, and R. Springmeyer. Bidirectional reflection functions from surface bump maps. *ACM Siggraph Computer Graphics*, 21:273–281, 1987.

[3] N. A. Carr, J. D. Hall, and J. C. Hart. GPU algorithms for radiosity and subsurface scattering. In *Proceedings of the ACM SIGGRAPH/EUROGRAPHICS conference on Graphics hardware*, pages 51–59. Eurographics Association, 2003.

[4] J. S. Cheung, E. Wang, E. H. Lo, and P. Z. Sun. Stratification of heterogeneous diffusion MRI ischemic lesion with kurtosis imaging evaluation of mean diffusion and kurtosis MRI mismatch in an animal model of transient focal ischemia. *Stroke*, 43(8):2252–2254, 2012.

[5] C. Correa and K.-L. Ma. Size-based transfer functions: A new volume exploration technique. *Visualization and Computer Graphics, IEEE Transactions on*, 14(6):1380–1387, 2008.

[6] D. B. Ennis, G. Kindlmann, I. Rodriguez, P. A. Helm, and E. R. McVeigh. Visualization of tensor fields using superquadric glyphs. *Magnetic Resonance in Medicine*, 53(1):169–176, 2005.

[7] N.-J. Gong, C.-S. Wong, C.-C. Chan, L.-M. Leung, and Y.-C. Chu. Correlations between microstructural alterations and severity of cognitive deficiency in alzheimer's disease and mild cognitive impairment: a diffusional kurtosis imaging study. *Magnetic Resonance Imaging*, 31(5):688 – 694, 2013.

[8] E. J. Grossman, Y. Ge, J. H. Jensen, J. S. Babb, L. Miles, J. Reaume, J. M. Silver, R. I. Grossman, and M. Inglese. Thalamus and cognitive impairment in mild traumatic brain injury: a diffusional kurtosis imaging study. *Journal of neurotrauma*, 29(13):2318–2327, 2012.

[9] M. Hlawitschka, Y. Hijazi, A. Knoll, and B. Hamann. Towards a high-quality visualization of higher-order reynolds glyphs for diffusion tensor imaging. In L. Linsen, H. Hagen, B. Hamann, and H.-C. Hege, editors, *Visualization in Medicine and Life Sciences II*, Mathematics and Visualization, pages 209–225. Springer Berlin Heidelberg, 2012.

[10] R. Huang and K.-L. Ma. RGVis: Region growing based techniques for volume visualization. In *Computer Graphics and Applications, 2003. Proceedings. 11th Pacific Conference on*, pages 355–363. IEEE, 2003.

[11] C. Y. Ip, A. Varshney, and J. JaJa. Hierarchical exploration of volumes using multilevel segmentation of the intensity-gradient histograms. *Visualization and Computer Graphics, IEEE Transactions on*, 18(12):2355–2363, 2012.

[12] M. O. Irfanoglu, L. Walker, S. Sammet, C. Pierpaoli, and R. Machiraju. Susceptibility distortion correction for echo planar images with non-uniform b-spline grid sampling: a diffusion tensor image study. In *Medical Image Computing and Computer-Assisted Intervention–MICCAI 2011*, pages 174–181. Springer, 2011.

[13] M. O. Irfanoglu, L. Walker, J. Sarlls, S. Marenco, and C. Pierpaoli. Effects of image distortions originating from susceptibility variations and concomitant fields on diffusion MRI tractography results. *NeuroImage*, 61(1):275 – 288, 2012.

[14] J. Jensen and J. Helpern. Quantifying non-Gaussian water diffusion by means of pulsed-field-gradient MRI. In *Proceedings of the 11th Annual Meeting of ISMRM*, volume 2154, 2003.

[15] J. H. Jensen and J. A. Helpern. MRI quantification of non-Gaussian water diffusion by kurtosis analysis. *NMR in Biomedicine*, 23(7):698–710, 2010.

[16] D. K. Jones. *Diffusion MRI theory, methods, and applications*. Oxford University Press, USA, 2011.

[17] J. Kautz, J. Snyder, and P.-P. J. Sloan. Fast Arbitrary BRDF Shading for Low-Frequency Lighting Using Spherical Harmonics. In *Eurographics Symposium on Rendering/Eurographics Workshop on Rendering Techniques*, pages 291–296, 2002.

[18] Y. Kim, A. Varshney, D. W. Jacobs, and F. Guimbretière. Mesh saliency and human eye fixations. *ACM Trans. Appl. Percept.*, 7(2):1–13, 2010.

[19] G. Kindlmann and D. Weinstein. Hue-balls and lit-tensors for direct volume rendering of diffusion tensor fields. In *Proceedings of the Conference on Visualization '99: Celebrating Ten Years*, VIS '99, pages 183–189, Los Alamitos, CA, USA, 1999. IEEE Computer Society Press.

[20] G. Kindlmann, D. Weinstein, and D. Hart. Strategies for direct volume rendering of diffusion tensor fields. *IEEE Transactions on Visualization and Computer Graphics*, 6(2):124–138, Apr. 2000.

[21] G. L. Kindlmann. Superquadric tensor glyphs. In *Joint Eurographics - IEEE TCVG Symposium on Visualization*, pages 147–154, 2004.

[22] G. L. Kindlmann and J. W. Durkin. Semi-automatic generation of transfer functions for direct volume rendering. In *Volume Visualization and Graphics*, pages 79–86, 1998.

[23] J. Kniss, G. Kindlmann, and C. Hansen. Multidimensional transfer functions for interactive volume rendering. *Visualization and Computer Graphics, IEEE Transactions on*, 8(3):270–285, Jul 2002.

[24] M. Lazar, J. H. Jensen, L. Xuan, and J. A. Helpern. Estimation of the orientation distribution function from diffusional kurtosis imaging. *Magnetic Resonance in Medicine*, 60:774–781, 2008.

[25] C. H. Lee, X. Hao, and A. Varshney. Light collages: Lighting design for effective visualization. In *IEEE Visualization*, pages 281 – 288, 2004.

[26] C. H. Lee, Y. Kim, and A. Varshney. Saliency-guided lighting. *IEICE Trans. on Information and Systems*, E92-D(2):369 – 373, February 2009.

[27] M. Levoy. Display of surfaces from volume data. *IEEE Computer Graphics and Applications*, 8:29–37, 1988.

[28] H. Lu, J. H. Jensen, A. Ramani, and J. A. Helpern. Three-dimensional characterization of non-gaussian water diffusion in humans using diffusion kurtosis imaging. *NMR in Biomedicine*, 19(2):236–247, 2006.

[29] E. B. Lum and K.-L. Ma. Lighting transfer functions using gradient aligned sampling. In *Proceedings of the conference on Visualization'04*, pages 289–296. IEEE Computer Society, 2004.

[30] M. J. Mohlenkamp. A Fast Transform for Spherical Harmonics. *Journal of Fourier Analysis and Applications*, 1997.

[31] K. T. Nguyen, A. Ynnerman, and T. Ropinski. Analyzing and reducing DTI tracking uncertainty by combining deterministic and stochastic approaches. In *Advances in Visual Computing*, pages 266–279. Springer, 2013.

[32] V. Prckovska, T. H. J. M. Peeters, M. Van Almsick, B. ter Haar Romeny, and A. Vilanova i Bartroli. Fused DTI/HARDI Visualization. *Visualization and Computer Graphics, IEEE Trans. on*, 17(10):1407–1419, 2011.

[33] P. Raab, E. Hattingen, K. Franz, F. E. Zanella, and H. Lanfermann. Cerebral gliomas: diffusional kurtosis imaging analysis of microstructural differences., 2010.

[34] A. Reichenbach, M. Hlawitschka, M. Tittgemeyer, and G. Scheuermann. *Choosing a Tractography Algorithm: On the Effects of Measurement Noise*, pages 115–128. Mathematics and Visualization. Springer International Publishing, 2014.

[35] P. Schlegel, M. Makhinya, and R. Pajarola. Extinction-Based Shading and Illumination in GPU Volume Ray-Casting. *IEEE Transactions on Visualization and Computer Graphics*, 17(12):1795–1802, 2011.

[36] T. Schultz. Topological features in 2D symmetric higher-order tensor fields. *Computer Graphics Forum*, 30(3):841–850, 2011.

[37] T. Schultz and G. Kindlmann. A maximum enhancing higher-order tensor glyph. *Computer Graphics Forum*, 29(3):1143–1152, 2010.

[38] T. Schultz and G. L. Kindlmann. Superquadric Glyphs for Symmetric Second-Order Tensors. *IEEE Transactions on Visualization and Computer Graphics*, 16:1595–1604, 2010.

[39] T. Schultz, L. Schlaffke, B. Schölkopf, and T. Schmidt-Wilcke. HiFiVE: A Hilbert Space Embedding of Fiber Variability Estimates for Uncertainty Modeling and Visualization. *Computer Graphics Forum*, 32(3pt1):121–130, 2013.

[40] T. Schultz, H. Theisel, and H.-P. Seidel. Topological visualization of brain diffusion MRI data. *IEEE Trans. on Visualization and Computer Graphics*, 13(6):1496–1503, 2007.

[41] G. Schussman and K.-L. Ma. Anisotropic volume rendering for extremely dense, thin line data. In *Proceedings of the conference on Visualization'04*, pages 107–114. IEEE Computer Society, 2004.

[42] A. Schwartzman, R. F. Dougherty, and J. E. Taylor. Cross-subject comparison of principal diffusion direction maps. *Magnetic Resonance in Medicine*, 53(6):1423–1431, 2005.

[43] F. X. Sillion, J. R. Arvo, S. H. Westin, and D. P. Greenberg. A global illumination solution for general reflectance distributions. In *ACM SIGGRAPH Computer Graphics*, volume 25, pages 187–196. ACM, 1991.

[44] P.-P. Sloan, J. Kautz, and J. Snyder. Precomputed radiance transfer for real-time rendering in dynamic, low-frequency lighting environments. In *ACM Transactions on Graphics (TOG)*, volume 21, pages 527–536. ACM, 2002.

[45] P. Staempfli, T. Jaermann, G. Crelier, S. Kollias, A. Valavanis, and P. Boesiger. Resolving fiber crossing using advanced fast marching tractography based on diffusion tensor imaging. *NeuroImage*, 30(1):110 – 120, 2006.

[46] Y. Tao, H. Lin, H. Bao, F. Dong, and G. Clapworthy. Structure-aware viewpoint selection for volume visualization. In *Visualization Symposium, Pacific Asia-Pacific*, pages 193–200, 2009.

[47] A. Tikhonova, C. D. Correa, and K.-L. Ma. An exploratory technique for coherent visualization of time-varying volume data. *Computer Graphics Forum*, 29(3):783–792, 2010.

[48] X. Tricoche, G. Kindlmann, and C.-F. Westin. Invariant crease lines for topological and structural analysis of tensor fields. *IEEE Trans. on Visualization and Computer Graphics*, 14(6):1627–1634, 2008.

[49] M. Van Almsick, T. H. J. M. Peeters, V. Prckovska, A. Vilanova, and B. ter Haar Romeny. GPU-Based Ray-Casting of Spherical Functions Applied to High Angular Resolution Diffusion Imaging. *Visualization and Computer Graphics, IEEE Trans. on*, 17(5):612–625, 2011.

[50] Y. Zhang and K.-L. Ma. Lighting Design for Globally Illuminated Volume Rendering. *Visualization and Computer Graphics, IEEE Transactions on*, 19(12):2946–2955, 2013.

[51] J. Zhuo, S. Xu, J. L. Proctor, R. J. Mullins, J. Z. Simon, G. Fiskum, and R. P. Gullapalli. Diffusion kurtosis as an in vivo imaging marker for reactive astrogliosis in traumatic brain injury. *NeuroImage*, 59(1):467 – 477, 2012.